46th AIAA/ASME/SAE/ASEE Joint Propulsion Conference & Exhibit
25 - 28 July 2010, Nashville, TN

AIAA 2010-6993

Axial Waves in Simulated Solid Rocket Motors

Nadim Zgheib* and Joseph Majdalani†
University of Tennessee Space Institute, Tullahoma, TN 37388

In this article, we consider the vorticoacoustic flowfield in a right-cylindrical porous chamber with uniform sidewall injection. Such configuration is often used to simulate the internal gaseous environment of a solid rocket motor (SRM). Assuming closed-closed acoustic conditions at both fore and aft ends of the domain, the introduction of small disturbances in the mean flow give rise to an axially traveling vortico-acoustically dominated wave structure that our study attempts to elucidate. Although this problem has been formulated before, it is reconsidered here in the context of WKB perturbation expansions in the reciprocal of the crossflow Reynolds number. This enables us to uncover multiple distinguished limits along with new asymptotic solutions that are presented for the first time. The WKB solutions are shown to exhibit a peculiar singularity that warrants the use of matched-asymptotic expansions to produce uniformly valid representations. Our solutions are obtained for any characteristic mean flow function satisfying Berman's similarity condition for porous tubes. They are also derived to an arbitrary level of precision using a recursive formulation that can reproduce each of the asymptotic solutions to any prescribed order. Finally, our solutions are verified numerically over a wide range of physical parameters and through limiting process approximations.

Nomenclature

a	=	radius of the chamber
L	=	length of the chamber
n	=	wave mode number
r	=	non-dimensional radial coordinate
R	=	crossflow Reynolds number
S	=	Strouhal number
u	=	acoustic wave velocity
x	=	non-dimensional axial coordinate
δ	=	small perturbation parameter
ε	=	inverse of the crossflow Reynolds number
ω	=	frequency of oscillations

Superscripts

c	=	composite solution
i	=	inner solution
o	=	outer solution
I	=	type I solution
II	=	type II solution
$\bar{}$	=	magnitude
$\hat{}$	=	irrotational acoustic wave
$\tilde{}$	=	solenoidal vorticity-induced wave
*	=	denotes dimensional quantities

*Graduate Research Assistant, Mechanical, Aerospace and Biomedical Engineering Department. Member AIAA.
†H. H. Arnold Chair of Excellence in Advanced Propulsion, Mechanical, Aerospace and Biomedical Engineering Department. Senior Member AIAA. Fellow ASME.

Subscripts

1	=	first order
m	=	acoustic oscillation mode number

I. Introduction

THE modeling of axially traveling, oscillatory waves in wall-transpiring porous tubes is pertinent to several engineering applications including flow filtration, pulmonary circulation, surface ablation, acoustic instability, and water hammering. In this study, the mean fluid motion is driven by injection along the tube's sidewall. As for the oscillatory waves, they may be the product of external excitation, resulting from the use of wave generators. The waves may also be stimulated internally in response to the inherent coupling with the tube's natural frequencies. The ensuing problem has been studied extensively and some examples are showcased in experimental investigations by Brown *et al*.,[1] Dunlap *et al*.,[2] Ma *et al*.,[3] and Barron *et al*.[4] These studies attempt to capture wave structures and potential instability during the burning of solid propellant grains.

It may be safely stated that the characterization of steady fluid motions in porous channels and tubes started with Berman.[5] Therein, Berman reduced the Navier-Stokes equations to a single, nonlinear, fourth-order ordinary differential equation (ODE) with four boundary conditions falling under the auspices of uniform wall injection or suction. His work opened up a new line of research inquiry in view of the substantial number of studies that emerged after the development of his similarity solution.

The steady flow problem becomes more challenging with the superposition of small amplitude sinusoidal waves. The presence of the waves gives rise to an axisymmetric oscillatory field that we wish to examine. The analysis at hand constitutes a crucial extension to a previous study by Majdalani[6] where he derives and discusses multiple asymptotic solutions in the context of two dimensional porous channels. Because the problem is laid out for a cylindrical geometry, the present configuration is more relevant to rocketry and other applications in which axisymmetric flows are induced. Following similar lines, asymptotic solutions of two types are captured via direct application of WKB expansions. Furthermore, matched-asymptotic expansions are used to overcome an essential singularity that arises near the centerline. Finally, a numerical formulation is presented to verify the analytical results.

II. Problem

This study seeks to investigate the possible forms of solutions that may be used to describe the unsteady velocity of a damped axially traveling wave inside a porous cylindrical tube of radius a and finite length $L >> a$. As shown by Majdalani and Roh,[7] the unsteady velocity of a vorticoacoustic wave, u_1, may be split into an irrotational part $\hat{u}$ and a solenoidal part $\tilde{u}$. This Helmholtz type decomposition can be expressed as

$$u_1(x,r,t) = \hat{u} + \tilde{u} \tag{1}$$

Using Euler's notation, the irrotational and the vortical responses may be specified as

$$\hat{u}(x,t) = \mathrm{i}\sin(\omega_m x)\exp(-\mathrm{i}\omega_m t) \tag{2}$$

$$\tilde{u}(x,r,t) = \overline{u}(x,r)\exp(-\mathrm{i}\omega_m t) \tag{3}$$

where $\overline{u}(x,r)$ represents the amplitude of the rotational component of the velocity,

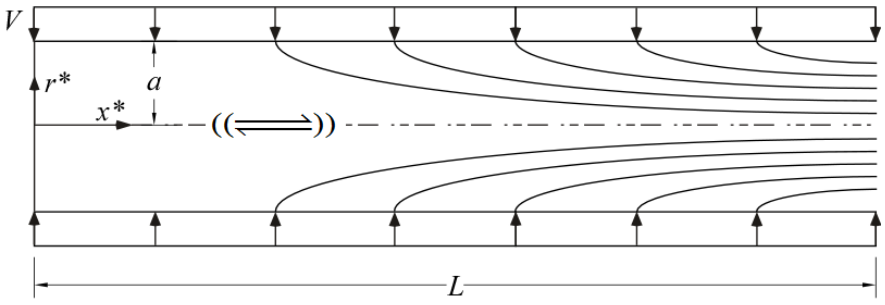

Figure 1. Right-cylindrical tube with injecting sidewall in which vorticoacoustic oscillations are sustained.

$$\overline{u}(x,r) = -\mathrm{i}\sum_{n=0}^{\infty}(-1)^n\left(\omega_m x\right)^{2n+1} R_n(r)\,/\,(2n+1)! \tag{4}$$

For the oscillatory field in a right-cylindrical porous tube, it was shown by Majdalani and Flandro[8] that the eigenfunction R_n, needed to capture the rapid radial variations in the rotational wave, may be determined from a complex second order ordinary differential equation

$$\varepsilon\frac{\mathrm{d}^2R_n}{\mathrm{d}r^2} + \frac{\left(\varepsilon+F\right)}{r}\frac{\mathrm{d}R_n}{\mathrm{d}r} + \left[\mathrm{i}S - 2(n+1)\frac{F'}{r}\right]R_n = 0; \quad 0\le r\le 1; \quad n\in\mathbb{N} \tag{5}$$

$$R_n(1) = 1 \text{ (no-slip), and } R_n'(0) = 0 \text{ (axisymmetry)} \tag{6}$$

Equation (5) represents a doubly perturbed asymptotic ODE with variable coefficients. It is controlled by ε, the reciprocal of the crossflow Reynolds number R, and by the Strouhal number S, which can be large especially at high oscillation modes. Furthermore, $F = F(r)$ corresponds to the base flow associated with a stream function $\psi = xF(r)$ satisfying Berman's spatial similarity. Following five decades of work on this problem, several solutions for $F(r)$ have been formulated over different ranges of R. These are also dependent on whether the fluid is injected or withdrawn at the sidewall (Terrill and Thomas,[9] and Terrill[10]). In relation to the present study, the two most pertinent injection-driven mean flow profiles are those examined in depth by Yuan and Finkelstein.[11] These are

$$F(r) = \begin{cases} r^2\left(2-r^2\right) + \mathcal{O}\left(10^{-2}Rr^2\right) & \left(10 < R < 100\right) \\ \sin\left(\frac{1}{2}\pi r^2\right) + \mathcal{O}\left(R^{-1}\right) & \left(R > 100\right) \end{cases} \tag{7}$$

In what is to follow, we will present asymptotic WKB expressions for Eq. (5) and then proceed to verify those numerically.

III. WKB Technique

Closed-form representations of the eigenfunction equation are intractable due to the variable coefficients that appear in the second and third terms. Moreover, the inherently stiff nature of the problem renders numerical solutions laborious, especially at large crossflow Reynolds numbers. In contrast, accurate asymptotic solutions that are simple to evaluate may be arrived at through direct application of the WKB technique. Accordingly, a formal WKB expansion may be introduced such that (cf. Bender and Orszag[12]):

$$R_n(r) = \exp\left(\delta^{-1}S_0 + S_1 + \delta S_2 + \delta^2 S_3 + \delta^3 S_4 + \ldots\right) \tag{8}$$

where δ is a small parameter and $S_j(r)$ must be determined sequentially for $j \ge 0$. Straightforward differentiation and substitution into Eq. (5) yields

$$\begin{cases} \varepsilon\left[\delta^{-1}S_0'' + S_1'' + \delta S_2'' + \delta^{-2}S_0'^2 + S_1'^2 + 2\delta^{-1}S_0'S_1' + 2S_0'S_2' + 2\delta S_1'S_2'\right] \\ +\dfrac{1}{r}\left(F+\varepsilon\right)\left(\delta^{-1}S_0' + S_1' + \delta S_2'\right) + \left[iS - 2(n+1)\dfrac{1}{r}F'\right] = 0 \end{cases} \tag{9}$$

Two distinguished limits are hence identified, namely $\delta = \varepsilon$ and $\delta = \sqrt{\varepsilon}$.

A. WKB Solution of Type I: $\delta = \sqrt{\varepsilon}$ and $S\sqrt{\varepsilon} = \mathcal{O}(1)$

Starting with Eq. (9) and replacing δ by $\sqrt{\varepsilon}$, we are left with

$$\frac{1}{\sqrt{\varepsilon}}\left(\frac{F}{r}S_0' + iS\sqrt{\varepsilon}\right) + \left(S_0'^2 + \frac{F}{r}S_1' - 2(n+1)\frac{1}{r}F'\right) + \sqrt{\varepsilon}\left(S_0'' + \frac{S_0'}{r} + 2S_0'S_1' + \frac{FS_2'}{r}\right) + \ldots = 0 \tag{10}$$

A leading order equation is immediately realized in the form of a first derivative,

$$S_0' = -\frac{riS\sqrt{\varepsilon}}{F} \tag{11}$$

It should be borne in mind that Eq. (11) does not constitute an Eikonal equation in the strict sense of the term. Typical Eikonal equations comprise a first derivative that is squared, which usually leads to dual solutions. Here, only one solution is prompted by the type I distinguished limit. As we turn our attention to the so-called transport

equation, the same departure from classic behavior is realized. In fact, the higher-order corrective functions, S_1 and S_2 become single valued and expressible by

$$S_1' = -\frac{rS_0'^2 - 2(n+1)F'}{F} \tag{12}$$

$$S_2' = -\frac{rS_0'' + 2rS_0'S_1' + S_0'}{F} \tag{13}$$

After carrying the solution to higher orders, a recursive relation is realized, namely,

$$S_{k+2}' = -\frac{1}{F}\left(S_k' + rS_k'' + r\sum_{i=0}^{k+1} S_i'S_{k+1-i}'\right) \qquad k \in \mathbb{N} \tag{14}$$

The type I solution may be constructed by integrating Eqs. (11), (12), and (13). We get

$$S_0(r) = -iS\sqrt{\varepsilon}\int_1^r \frac{x}{F(x)}\,\mathrm{d}x \tag{15}$$

$$S_1(r) = \xi\int_1^r \frac{x^3}{F^3(x)}\,\mathrm{d}x + \ln\left[\frac{F(r)}{F(1)}\right]^{2n+2}; \quad \xi = \varepsilon S^2 \tag{16}$$

$$S_2(r) = \mathrm{i}S\sqrt{\varepsilon}\left\{(2n+\tfrac{3}{2})\left[1 - r^2F^{-2}(r)\right] + (4n+5)\int_1^r \left[x \,/\, F^2(x)\right]\mathrm{d}x + 2\xi\int_1^r \left[x^5 \,/\, F^5(x)\right]\mathrm{d}x\right\} \tag{17}$$

By substituting the above expressions into Eq. (8), we obtain the leading order type I solution

$$R_n^I(r) = F^{2n+2}\exp\left(\zeta_0 - \mathrm{i}\Phi_0 - \mathrm{i}\Phi_1^n\right) + O(\varepsilon) \tag{18}$$

where

$$\begin{cases} \zeta_0 = \xi\int_1^r \frac{x^3}{F^3(x)}\,\mathrm{d}x; \quad \xi = \varepsilon S^2; \quad \Phi_0 = S\int_1^r \frac{x}{F(x)}\,\mathrm{d}x; \\ \Phi_1^n = -\varepsilon S\left\{(2n+\frac{3}{2})\left[1 - r^2F^{-2}(r)\right] + (4n+5)\int_1^r \left[x \,/\, F^2(x)\right]\mathrm{d}x + 2\xi\int_1^r \left[x^5 \,/\, F^5(x)\right]\mathrm{d}x\right\} \end{cases} \tag{19}$$

B. WKB Solution of Type II: $\delta = \varepsilon$ and $\varepsilon S = \mathcal{O}(1)$

Bearing in mind that $\varepsilon S = \mathcal{O}(1)$, we may substitute Eq. (8) back into Eq. (5) and collect terms of the same order in ε. We get

$$\begin{cases} \frac{1}{\varepsilon}\left(S_0'^2 + \frac{F}{r}S_0' + i\varepsilon S\right) + \left[S_0'' + 2S_0'S_1' + \frac{1}{r}S_0' + \frac{F}{r}S_1' - 2(n+1)\frac{1}{r}F'\right] \\ \qquad + \varepsilon\left(S_1'' + S_1'^2 + 2S_0'S_2' + \frac{S_1'}{r} + \frac{FS_2'}{r}\right) + \ldots = 0 \end{cases} \tag{20}$$

Since Eq. (20) must be satisfied for all values of ε, the quantities inside the parentheses must sequentially vanish, starting with the lowest order. Resolution of the ε multipliers may hence be continued until a desired order is reached. For the type II case, a conventional Eikonal equation is captured, namely,

$$S_0'^2 + \frac{F}{r}S_0' + i\varepsilon S = 0 \tag{21}$$

Its dual roots are given by

$$\begin{cases} S_{01} = -\int_1^r \frac{1}{2x}\left[F(x) + \sqrt{F(x)^2 - 4iS_t\varepsilon x^2}\right]\mathrm{d}x \\ S_{02} = -\int_1^r \frac{1}{2x}\left[F(x) - \sqrt{F(x)^2 - 4iS_t\varepsilon x^2}\right]\mathrm{d}x \end{cases} \tag{22}$$

Due to the quadratic nature of the Eikonal equation and the duality of its roots, S_{01} and S_{02}, two conjugate solutions will be obtained for each of the higher-order corrections S_1, S_2, S_3 and so on. Each of these values will correspond to either S_{01} or S_{02}.

At $\mathcal{O}(1)$, the transport equation may be solved for S_1 with the outcome,

$$S_1 = -\int_1^r \frac{xS_0''(x) + S_0'(x) - 2(n+1)F'(x)}{2xS_0'(x) + F(x)}\,\mathrm{d}x \tag{23}$$

At $\mathcal{O}(\varepsilon)$, S_2 reduces to

$$S_2 = -\int_1^r \frac{xS_1'(x) + xS_1'^2(x) + S_1'(x)}{2xS_0'(x) + F(x)}\,\mathrm{d}x \tag{24}$$

Higher orders may be similarly achieved. After some effort, a recursive relation is developed to help reproduce the successive corrections,

$$S_{k+3} = -\int_1^r \left(F + 2rS_0'\right)^{-1}\left(S_{k+2}' + xS_{k+2}'' + 2xS_1'S_{k+2}' + x\sum_{i=1}^{k} S_{i+1}'S_{k+2-i}'\right)\mathrm{d}x; \qquad k \in \mathbb{N}^* \tag{25}$$

This recursive formula is valid for any order. In most practical applications, however, no more than three terms are needed to accurately describe the longitudinal wave behavior.

By substituting Eqs. (22), (23), and (24) into Eq. (8), the type II solution R_n^{II} may be arrived at. The linearity of Eq. (5) warrants the inclusion of both conjugates in Eq. (22) and higher-order terms. We hence retrieve

$$R_n^{II} = C_1 \exp\left(\delta^{-1}S_{01} + S_{11} + \delta S_{21}\right) + C_2 \exp\left(\delta^{-1}S_{02} + S_{12} + \delta S_{22}\right) \tag{26}$$

$$\begin{cases} S_{11} = -\int_1^r \dfrac{xS_{01}''\left(x\right) + S_{01}'\left(x\right) - 2(n+1)F'(x)}{2xS_{01}'(x) + F(x)}\,\mathrm{d}x \\ S_{12} = -\int_1^r \dfrac{xS_{02}''(x) + S_{02}'(x) - 2(n+1)F'(x)}{2xS_{02}'(x) + F(x)}\,\mathrm{d}x \end{cases} \tag{27}$$

$$\begin{cases} S_{21} = -\int_1^r \dfrac{xS_{11}''(x) + xS_{11}'^2(x) + S_{11}'(x)}{2xS_{01}'(x) + F(x)}\,\mathrm{d}x \\ S_{22} = -\int_1^r \dfrac{xS_{12}''(x) + xS_{12}'^2(x) + S_{12}'(x)}{2xS_{02}'(x) + F(x)}\,\mathrm{d}x \end{cases} \tag{28}$$

At this juncture, the problem's boundary conditions may be applied to determine the constants of integration. In order to secure Eq. (6) and ensure boundedness throughout the domain, we take $C_1 = 0$ and $C_2 = 1$. The type II approximation reduces to

$$R_n^{II}\left(r\right) = \exp\left(\varepsilon^{-1}S_{02} + S_{12} + \varepsilon S_{22}\right) + \mathcal{O}(\varepsilon^2) \tag{29}$$

For the type I solution, in both the rectangular channel[6] and the cylindrical tube, the value of R_n^I at the core alternates between zero and infinity, depending on the order at which the solution is truncated. The solution suddenly becomes unbounded at even orders in ε, $R_n^I \to \infty$ as $r \to 0$. However, for odd orders in ε, the solution appears to be well behaved, $R_n^I \to 0$ as $r \to 0$. In reality, the numerical solution suggests that neither outcome is correct; R_n rather possesses an asymptotically small value at $r = 0$ that may be explicitly estimated. As for the type II solution, the cylindrical case exhibits a unique singular behavior at the centerline with a pattern that again alternates between zero and infinity every four orders in ε. Contrary to the cylindrical case, the type II channel solution remains uniformly valid and singularity-free throughout the entire domain. Moreover, the type II solution leads to a generally quasi-analytical form for some mean flow functions that preclude the explicit integration of Eqs. (22), (23), and (24). For $F(r) = \sin(\frac{1}{2}\pi r^2)$ these have to be integrated numerically. This is atypical of the WKB type I formulation which has engendered a closed-form analytical solution for this study as well as for the porous channel flow analog.[6]

Figure 2 has more to offer than just validating the favorable agreement between the type II axial velocity and its numerical counterpart. Not only does it display the role of the Strouhal and the injection Reynolds numbers in controlling the intensity of oscillations, it also exemplifies the importance of the viscous parameter εS^2. Maintaining a constant penetration number $S_p = \left(\varepsilon S^2\right)^{-1} = R / S^2$ results in a constant penetration depth irrespective of the operating parameters. Note that the fulfillment of the no-slip condition is observed where the irrotational component of the wave counterbalances its rotational counterpart at $r = 0$. On the other hand these components augment each other very close to the surface in what is known as the annular effect, first observed by

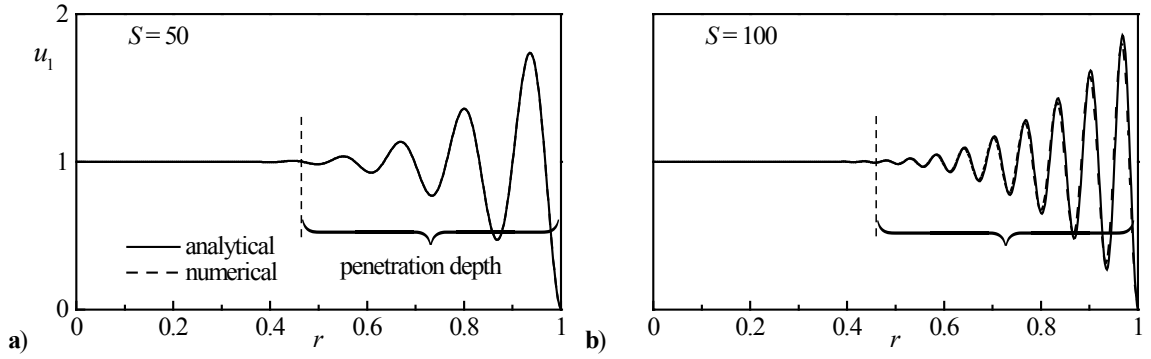

Figure 2. Numerical and analytical WKB type II solutions for $F = \sin(\frac{1}{2}\pi r^2)$, $\varepsilon S^2 = 5$, $\omega_m t = \pi / 2$, $x / L = \frac{1}{2}$, and a Strouhal number of a) $S = 50$ and b) $S = 100$.

Richardson and Tyler.[13] This phenomenon appears in both porous and non-porous ducts in which fluid motion is rapidly alternating.[6]

IV. Matched-Asymptotic Expansions

In order to overcome the core singularity in the type II solution, the method of matched-asymptotic expansions will be used. This technique enables us to split the domain into an inner layer corresponding to the region of non-uniformity, and an outer region where the solution is well behaved. A suitable approximation is then constructed for each of these regions, and these local expansions are subsequently matched over their overlap region and combined into a composite solution that stays uniformly valid over the entire domain of interest.

A. Outer Approximation

Our leading-order outer solution may be obtained directly from Eq. (5) by suppressing all terms that involve the primary perturbation parameter ε. This basic cancellation leaves us with

$$\frac{F}{r}\frac{\mathrm{d}R_n^o}{\mathrm{d}r} + \left[iS - 2(n+1)\frac{1}{r}F'\right]R_n^o = 0; \quad R_n^o(1) = 1 \tag{30}$$

where R_n^o refers to an outer expansion. Equation (30) may be readily solved to obtain

$$R_n^o(r) = \sin\left(\tfrac{1}{2}\pi r^2\right)^{2+2n} \tan\left(\tfrac{1}{4}\pi r^2\right)^{-iS/\pi} \tag{31}$$

To segregate the contribution of the outer solution in the core region, we take the limit as $r \to 0$. This operation renders the inner expansion of the outer solution, or $(R_n^o)^i$:

$$(R_n^o)^i = 2^{\mathrm{i}S/\pi}\left(\tfrac{1}{2}\pi r^2\right)^{2+2n-\mathrm{i}S/\pi} \tag{32}$$

The determination of a compact outer solution will prove to be instrumental in retrieving an expression for the inner expansion. This aspect will be illustrated next.

B. Inner Core Approximation

Near the core, one can express the mean flow characteristic function as $F = \alpha r^2$, where $\alpha = \pi / 2$ mimics large injection profiles as $r \to 0$. Equation (5) can then be subjected to a double variable transformation of the type

$$\begin{cases} \chi = r\sqrt{\alpha / \varepsilon} \\ R_n^i(\chi) = f(\chi)\exp\left(-\tfrac{1}{4}\chi^2\right) \end{cases} \tag{33}$$

At the outset, the rescaled Eqs. (5) and (6) become

$$\frac{\mathrm{d}^2 f}{\mathrm{d}\chi^2} + \frac{1}{\chi}\frac{\mathrm{d}f}{\mathrm{d}\chi} + \left(-5 - 4n + \mathrm{i}S\alpha^{-1} - \tfrac{1}{4}\chi^2\right)f = 0; \qquad \frac{\mathrm{d}f(0)}{\mathrm{d}\chi} = 0 \tag{34}$$

Table 1. Numerical and asymptotic solutions at $\mathcal{O}(\varepsilon^2)$ using $S = 10$, $R = 10^3$, $n = 0$, and $F = \sin(\frac{1}{2}\pi r^2)$

r	WKB I	WKB II	Numerical	Composite
0.00	∞	∞	1.37×10^{-6}	1.39×10^{-6}
0.05	∞	-0.000014	-0.000014	-0.000014
0.10	-0.000259	0.000018	0.000017	0.000020
0.15	0.000998	0.000907	0.000908	0.000924
0.20	-0.001189	-0.001189	-0.001188	-0.001264
0.25	-0.008467	-0.008424	-0.008425	-0.008614
…				
0.75	-0.418811	-0.418824	-0.418824	-0.413059
0.80	-0.223137	-0.223143	-0.223143	-0.205649
0.85	0.115410	0.115411	0.115411	0.143387
0.90	0.517774	0.517780	0.517780	0.550385
0.95	0.857983	0.857989	0.857989	0.885910
1.00	1.000000	1.000000	1.000000	1.013719

Note that only the boundary condition in the core region is transformed. The second boundary condition must be evaluated in the farfield to the extent of reproducing the inner expansion of the outer solution, $(R_n^o)^i$. Equation (34) may be readily manipulated to extract

$$f\left(\chi\right) = c_0\sqrt{2}\exp\left(\tfrac{1}{4}\chi^2\right)L_\eta\left(-\tfrac{1}{2}\chi^2\right); \quad \eta = 2 + 2n - \tfrac{1}{2}\mathrm{i}\alpha^{-1}S \tag{35}$$

where c_0 is a constant that must be determined through a matching operation between the inner and outer solutions in their overlap region. In the above, the special function $L_y(x)$ represents the Laguerre polynomial which is defined in terms of $\Phi\left(a,b,x\right)$, the Kummer function of the first kind.[14] These functions are given by

$$L_y(x) = \exp(x)\Phi(y+1,1,-x); \qquad \Phi(a,b,x) = \sum_{k=0}^{\infty}\frac{a_k}{b_k}\frac{z^k}{k!} \tag{36}$$

At this stage, Prandtl's matching principle may be implemented. Accordingly, the inner limit of the outer solution $(R_n^o)^i$ must be equated to the outer limit of the inner solution. Finding the latter requires the use of the large-x approximation of the Kummer function Φ,

$$\Phi(a,b,x) = \frac{\Gamma(b)}{\Gamma(a)}\exp(x)x^{a-b}\left[1+\mathcal{O}(x^{-1})\right]; \quad x\to\infty \tag{37}$$

This expression enables us to convert Eq. (35) into

$$f\left(\chi\right) = c_0\sqrt{2}\,\Phi(3+2n-\mathrm{i}S/\pi,1,\tfrac{1}{2}\chi^2) \sim \frac{c_0\sqrt{2}\;\Gamma(1)}{\Gamma(3+2n-\mathrm{i}S/\pi)}\exp(\tfrac{1}{2}\chi^2)\left(\tfrac{1}{2}\chi^2\right)^{2+2n-\mathrm{i}S/\pi} \tag{38}$$

whence, based on Eq. (33), we get

$$(R_n^i)^o = \frac{c_0\sqrt{2}}{\Gamma(3+2n-\mathrm{i}S/\pi)}\exp\left(\frac{\pi r^2}{8\varepsilon}\right)\left(\frac{\pi r^2}{4\varepsilon}\right)^{2+2n-\mathrm{i}S/\pi} \tag{39}$$

Matching and retrieving the inner solution at order ε yields

$$R_n^i(r) = \Gamma\left(3+2n-\mathrm{i}S/\pi\right)2^{2+2n}\varepsilon^{2+2n-\mathrm{i}S/\pi}\,L_\eta\left(-\tfrac{1}{4}\pi R r^2\right) \tag{40}$$

Finally, the composite solution $R^c = R^o + R^i - \left(R^i\right)^o$ may be constructed viz.

$$R^{\mathrm{c}}(r) = \begin{cases}\sin\left(\frac{1}{2}\pi r^2\right)^{2+2n}\tan\left(\frac{1}{4}\pi r^2\right)^{-iS/\pi} - 2^{\mathrm{i}S/\pi}\left(\frac{1}{2}\pi r^2\right)^{2+2n-\mathrm{i}S/\pi} \\ +\Gamma\left(3+2n-\mathrm{i}S/\pi\right)2^{2+2n}\varepsilon^{2+2n-\mathrm{i}S/\pi}\,L_\eta\left(-\frac{1}{4}\pi R r^2\right)\end{cases} \tag{41}$$

A comparison between the second-order asymptotic approximations and numerical predictions is presented in Table 1. By focusing attention on the domain's endpoints, it is interesting to see how well the composite

approximation matches the numerical value at the origin. Meanwhile, both types of WKB expansions fail at that truncation order by providing an infinitely large magnitude as $r \to 0$. As we move away from the origin, the WKB approximations begin to outperform, as they should, the composite expansion from which the outer solution may be recovered asymptotically in ε. Thus, unless ε is exceedingly small, the ability of the composite solution to outperform the outer solution in the outer region will remain limited. This explains the small discrepancy in the composite approximation near $r = 1,$ a weakness to which the WKB solutions remain immune.

V. Numerical Solution

The numerical solution presents its own challenges. The position of ε multiplying the highest derivative creates significant numeric instability for large, expected values of R. To complicate matters further, the r^{-1} factors in the coefficients pose potential problems around the centerline, $r = 0$.

If we consider a solution of the form

$$g(r,t) = R_n(r)e^{-\mathrm{i}T}, \quad T = \omega_m t \tag{42}$$

then

$$\frac{\partial g}{\partial r} = R_n'(r)e^{-\mathrm{i}T}, \quad \frac{\partial^2 g}{\partial r^2} = R_n''(r)e^{-\mathrm{i}T}, \quad \frac{\partial g}{\partial T} = -\mathrm{i}R_n(r)e^{-\mathrm{i}T} \tag{43}$$

The above expressions can be substituted into Eq. (5) and simplified through multiplication by $e^{-\mathrm{i}T}$. We are left with

$$\varepsilon\frac{\partial^2 g}{\partial r^2} + \frac{1}{r}(F+\varepsilon)\frac{\partial g}{\partial r} - \frac{2}{r}(n+1)F'g = S\frac{\partial g}{\partial T} \tag{44}$$

The same transformation would then be applied to the boundary conditions in Eq. (6),

$$g(1,t) = e^{-\mathrm{i}T}; \qquad \frac{\partial g}{\partial r}(0,t) = 0 \tag{45}$$

By allowing for sinusoidal oscillations in time, Eq. (44) may be converted into a set of coupled ODEs. This is achieved by taking

$$g(r,t) = g_1(r)\sin T - g_2(r)\cos T \tag{46}$$

This step returns the reduced set of linear equations with complex boundary conditions

$$\begin{cases} g_1'' = \left[\dfrac{2}{r}(n+1)F'g_1 - \dfrac{1}{r}\Big(F+\varepsilon\Big)g_1' + Sg_2\right]R \\ g_2'' = \left[\dfrac{2}{r}(n+1)F'g_2 - \dfrac{1}{r}\Big(F+\varepsilon\Big)g_2' - Sg_1\right]R \end{cases}; \qquad \begin{cases} g_1(1) = -i; & g_2(1) = -1 \\ g_1'(0) = 0; & g_2'(0) = 0 \end{cases} \tag{47}$$

The wave motion can now be reproduced from Eq. (1),

$$\begin{cases} u_1 = \sin(\omega_m x)\sin(\omega_m t) + \mathrm{i}\sin(\omega_m x)\cos(\omega_m t) \\ \qquad -\mathrm{i}\displaystyle\sum_{n=0}^{\infty}(-1)^n\frac{(\omega_m x)^{2n+1}}{(2n+1)!}\Big(g_1\sin\omega_m t - g_2\cos\omega_m t\Big) \end{cases} \begin{cases} g_1(1) = -i; & g_2(1) = -1 \\ g_1'(0) = 0; & g_2'(0) = 0 \end{cases} \tag{48}$$

Recognizing that only the real part in Eq. (48) is useful, we let $f_1(r) = \Re\big[\mathrm{i}g_1(r)\big]$, $f_2(r) = \Re\big[\mathrm{i}g_2(r)\big]$, and recast the problem in the real domain where

$$u_1 = \sin(\omega_m x)\sin(\omega_m t) - \sum_{n=0}^{\infty}(-1)^n\frac{(\omega_m x)^{2n+1}}{(2n+1)!}\Big(f_1\sin\omega_m t - f_2\cos\omega_m t\Big) \tag{49}$$

Here f_1 and f_2 must be obtained from a set of real coupled ODEs, namely,

$$\begin{cases} f_1'' = \left[\dfrac{2}{r}(n+1)F'f_1 - \dfrac{1}{r}\Big(F+\varepsilon\Big)f_1' + Sf_2\right]R \\ f_2'' = \left[\dfrac{2}{r}(n+1)F'f_2 - \dfrac{1}{r}\Big(F+\varepsilon\Big)f_2' - Sf_1\right]R \end{cases} \quad \text{with} \quad \begin{cases} f_1(1) = 1, & f_2(1) = 0 \\ f_1'(0) = 0, & f_2'(0) = 0 \end{cases} \tag{50}$$

In short, the temporal wave velocity is obtained by solving Eq. (50) and substituting the results back into Eq. (49).

VI. Results and Discussion

Inasmuch as this problem resembles its porous channel flow analog, mathematically it is quite different. For our cylindrical geometry, the $1/r$ term multiplying R' in Eq. (5) changes the character of the differential equation, especially near the core.

Away from the core, the WKB solutions are well behaved and accurate. However, their inherent singularity at the centerline must be carefully treated. In this study, matched-asymptotic expansions are used to arrive at a uniformly valid composite solution capable of capturing the small amplitude wave velocity at $r = 0$. Nevertheless, the increased accuracy associated with the composite solution at the core comes at the expense of a small residual error plaguing the outer expansion. In the process of formulating a composite solution, an inner core test function $F = \frac{1}{2}\pi r^2$ had to be used to arrive at a closed-form analytical solution. Even though the test function constitutes an excellent approximation near the core, it deteriorates, thus becoming the source of discrepancy in the outer domain. At the outset, we now have a choice between two analytical approximations. One that is accurate away from the center (WKB solutions) albeit oblivious of the small core correction, and another (composite solution), that excels where the WKB fails, but falls short where the WKB approximation performs superbly well, away from the centerline.

Figure 3 depicts the modulus of the time-dependent velocity throughout the entire tube for multiple mode numbers. When the oscillation mode number m is increased, the magnitude of the temporal velocity appears to follow the spatial mode shape of the irrotational component of the wave in Eq. (2). For the first mode, the magnitude of the wave grows from a minimum at the tube's head-end to a maximum, midway into the chamber, where the magnitude of the sinusoidal wave is largest. The penetration depth of the wave, for all modes, continues to increase along the tube as a result of the convection of the unsteady vorticity. When higher mode numbers are considered, $m \geq 2$, we notice the presence of velocity nodes, points were the vortical velocity contribution vanishes. The number and location of these nodes depends on the mode number and are described in a technical note by Majdalani.[15]

VII. Conclusions

This article investigates the behavior of the oscillatory motion associated with the Taylor-Culick flowfield after being subjected to small pressure oscillations in a porous tube with an injecting sidewall. Particular to this

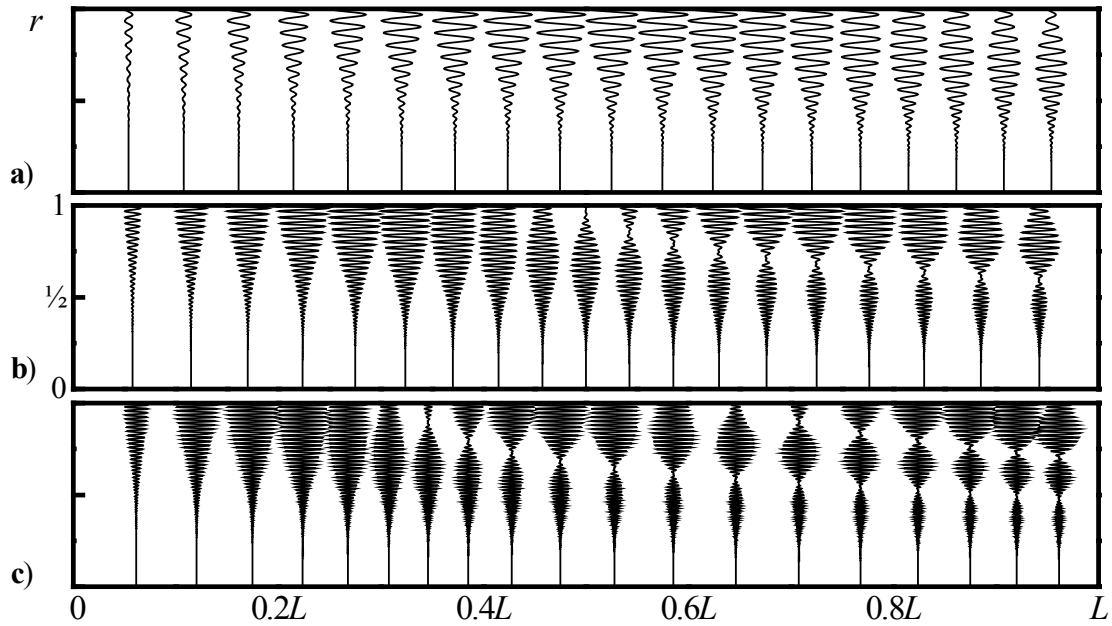

Figure 3. WKB type II magnitude of the temporal velocity for the first three oscillation modes using $F = \sin(\frac{1}{2}\pi r^2)$, $R = 10^4$, and $S = 100m$, with $m = 1, 2, 3$ corresponding to parts a), b), and c), respectively.

investigation, two forms of the WKB solution are derived and presented to arbitrary order. Both types show excellent agreement with the numerical solution; however, they fail to capture the behavior at the centerline. Through a series of transformations, matched-asymptotic expansions are used to develop a composite, singularity-free approximation valid over the entire domain. The matched-asymptotic expansion technique serves three objectives: (a) it demonstrates that a uniformly valid asymptotic solution can be obtained over the entire domain; (b) it validates to several decimal places the calculated numerical value at the centerline; and (c) it illustrates Prandtl's principle that proposes matching with supplementary expansions. In future work, it is hoped that the vortico-acoustic wave will be investigated in porous channels and tubes in the presence of headwall injection. It is also hoped that the problem of traveling, radial and tangential, waves will be considered in short chambers in which transverse wave interactions dominate.

Acknowledgments

This project was partly funded by the National Science Foundation through grant No. CMMI-0928762.

References

[1]Brown, R. S., Blackner, A. M., Willoughby, P. G., and Dunlap, R., "Coupling between Acoustic Velocity Oscillations and Solid Propellant Combustion," *Journal of Propulsion and Power,* Vol. 2, No. 5, 1986, pp. 428-437. doi: 10.2514/3.22925

[2]Dunlap, R., Blackner, A. M., Waugh, R. C., Brown, R. S., and Willoughby, P. G., "Internal Flow Field Studies in a Simulated Cylindrical Port Rocket Chamber," *Journal of Propulsion and Power,* Vol. 6, No. 6, 1990, pp. 690-704. doi: 10.2514/3.23274

[3]Ma, Y., Van Moorhem, W. K., and Shorthill, R. W., "Experimental Investigation of Velocity Coupling in Combustion Instability," *Journal of Propulsion and Power,* Vol. 7, No. 5, 1991, pp. 692-699. doi: 10.2514/3.23381

[4]Barron, J., Majdalani, J., and Van Moorhem, W. K., "A Novel Investigation of the Oscillatory Field over a Transpiring Surface," AIAA Paper 98-2694, June 1998.

[5]Berman, A. S., "Laminar Flow in Channels with Porous Walls," *Journal of Applied Physics,* Vol. 24, No. 9, 1953, pp. 1232-1235. doi: 10.1063/1.1721476

[6]Majdalani, J., "Multiple Asymptotic Solutions for Axially Travelling Waves in Porous Channels," *Journal of Fluid Mechanics,* Vol. 636, No. 1, 2009, pp. 59-89. doi: 10.1017/S0022112009007939

[7]Majdalani, J., and Roh, T. S., "The Oscillatory Channel Flow with Large Wall Injection," *Proceedings of the Royal Society of London, Series A,* Vol. 456, No. 1999, 2000, pp. 1625-1657. doi: 10.1098/rspa.2000.0579

[8]Majdalani, J., and Flandro, G. A., "The Oscillatory Pipe Flow with Arbitrary Wall Injection," *Proceedings of the Royal Society of London, Series A,* Vol. 458, No. 2023, 2002, pp. 1621-1651. doi: 10.1098/rspa.2001.0930

[9]Terrill, R. M., and Thomas, P. W., "On Laminar Flow through a Uniformly Porous Pipe," *Applied Scientific Research,* Vol. 21, No. 1, 1969, pp. 37-67. doi: 10.1007/BF00411596

[10]Terrill, R. M., "Laminar Flow in a Porous Tube," *ASME Journal of Fluids Engineering,* Vol. 105, No. 3, 1983, pp. 303-307. doi: 10.1115/1.3240992

[11]Yuan, S. W., and Finkelstein, A. B., "Laminar Pipe Flow with Injection and Suction through a Porous Wall," *Transactions of the American Society of Mechanical Engineers: Journal of Applied Mechanics,* Vol. 78, No. 3, 1956, pp. 719-724.

[12]Bender, C. M., and Orszag, S. A., *Advanced Mathematical Methods for Scientists and Engineers*, McGraw-Hill, New York, 1978.

[13]Richardson, E. G., and Tyler, E., "The Transverse Velocity Gradient near the Mouths of Pipes in Which an Alternating or Continuous Flow of Air Is Established," *Proceedings of the Physical Society,* Vol. 42, No. 1, 1929, pp. 1-15. doi: 10.1088/0959-5309/42/1/302

[14]Abramowitz, M., and Stegun, I. A., *Handbook of Mathematical Functions*, National Bureau of Standards, New York, 1964.

[15]Majdalani, J., "The Boundary Layer Structure in Cylindrical Rocket Motors," *AIAA Journal,* Vol. 37, No. 4, 1999, pp. 505-508. doi: 10.2514/2.742